The Journal of Chemical Physics

Solid effect in magic angle spinning dynamic nuclear polarization

Cite as: J. Chem. Phys. **137**, 054201 (2012); https://doi.org/10.1063/1.4738761
Submitted: 13 April 2012 . Accepted: 09 July 2012 . Published Online: 03 August 2012

Björn Corzilius, Albert A. Smith, and Robert G. Griffin

Solid effect in magic angle spinning dynamic nuclear polarization

Björn Corzilius, Albert A. Smith, and Robert G. Griffin
Francis Bitter Magnet Laboratory and Department of Chemistry, Massachusetts Institute of Technology, 77 Massachusetts Avenue, Cambridge, Massachusetts 02139, USA

(Received 13 April 2012; accepted 9 July 2012; published online 3 August 2012)

For over five decades, the solid effect (SE) has been heavily utilized as a mechanism for performing dynamic nuclear polarization (DNP). Nevertheless, it has not found widespread application in contemporary, high magnetic field DNP experiments because SE enhancements display an ω_0^{-2} field dependence. In particular, for nominally forbidden zero and double quantum SE transitions to be partially allowed, it is necessary for mixing of adjacent nuclear spin states to occur, and this leads to the observed field dependence. However, recently we have improved our instrumentation and report here an enhancement of $\varepsilon = 91$ obtained with the organic radical trityl (OX063) in magic angle spinning experiments performed at 5 T and 80 K. This is a factor of 6-7 higher than previous values in the literature under similar conditions. Because the solid effect depends strongly on the microwave field strength, we attribute this large enhancement to larger microwave field strengths inside the sample volume, achieved with more efficient coupling of the gyrotron to the sample chamber. In addition, we develop a theoretical model to explain the dependence of the buildup rate of enhanced nuclear polarization and the steady-state enhancement on the microwave power. Buildup times and enhancements were measured as a function of ^{1}H concentration for both trityl and Gd-DOTA. Comparison of the results indicates that for trityl the initial polarization step is the slower, rate-determining step. However, for Gd-DOTA the spread of nuclear polarization via homonuclear ^{1}H spin diffusion is rate-limiting. Finally, we discuss the applicability of the solid effect at fields > 5 T and the requirements to address the unfavorable field dependence of the solid effect. © *2012 American Institute of Physics*. [http://dx.doi.org/10.1063/1.4738761]

I. INTRODUCTION

Dynamic nuclear polarization (DNP) is a technique capable of enhancing the sensitivity of nuclear magnetic resonance (NMR) by several orders of magnitude. DNP was first proposed by Overhauser[1] and confirmed experimentally by Carver and Slichter[2] for the case of a conducting solid with mobile electrons. Subsequently, additional DNP mechanisms emerged for insulating solids, the first being solid effect (SE) (Refs. 3–5) which relies on the availability of a narrow line polarizing agent. Thereafter, two DNP mechanisms which greatly differ from the solid effect were discovered; namely, the cross effect (CE) (Refs. 6–10) and thermal mixing (TM) (Ref. 11). Both the CE and TM rely on multi-spin interactions and are active when the breadth of the EPR spectrum matches or exceeds the nuclear Larmor frequency of the nucleus being polarized.

The SE utilizes mixing of electronic and nuclear spin states mediated by the non-secular electron-nuclear coupling and microwave irradiation to excite nominally "forbidden" zero or double quantum (ZQ/DQ) transitions leading to enhanced nuclear polarization.[12] In order to selectively excite the transition leading to either positive or negative nuclear enhancements, both forbidden transitions must be well separated in the field/frequency domain.[13] This is the case when both the homogeneous and inhomogeneous linewidth of the polarizing agent's electron paramagnetic resonance (EPR) signal is smaller than twice the Larmor frequency of the nucleus to be polarized. Thus, "narrow-linewidth" radicals such as trityl (Ref. 14) or BDPA (Ref. 15) are effective polarizing agents for the solid effect.[16]

More than 50 years ago Jeffries *et al.* and Abragam independently performed the first experiments based on the SE.[3–5] These early efforts were conducted at low magnetic field (0.3–1.4 T) where the inherent efficiency of the solid effect is relatively high due to the favorable mixing of electronic and nuclear spin states. Furthermore, high-power microwave sources and cavities operating in the 10-40 GHz frequency range were readily available, and considerable attention was focused on understanding and implementing SE experiments. However, with the contemporary transition of DNP to high magnetic fields, the SE has played a minor role in comparison to the generally more efficient cross effect using biradical polarizing agents.[16–18] The reason for this has been the understanding that, due to the ω_0^{-2} field dependence, the enhancements will not be large which appears to have been confirmed experimentally. For example, *in situ* magic angle spinning (MAS) experiments performed by Hu *et al.* at 5 T (140 GHz) yielded $\varepsilon \approx$ 10-15.[19] In contrast, with biradicals as polarizing agents, enhancements of ∼200 were achieved with relatively low radical concentrations of 10-20 mM.[20] Accordingly, these results stimulated development of methods focused on optimizing DNP parameters and polarizing agents for the cross effect.[16,17,19,21–27] The exceptions to this statement are the theoretical discussions by Vega and co-workers.[28–30]

Despite the modest enhancements, we have continued to investigate DNP experiments with the SE, and have recently

shown that enhancements of 94 are feasible at 5 T and 80 K using trityl as the polarizing agent. These experiments were performed with a microwave cavity in order to increase the microwave field strength inside the sample volume.[31] These results suggested that if we could efficiently couple the microwaves to the sample in MAS experiments, similar enhancements should be observed. In this paper we show that this is indeed the case for MAS experiments performed without a resonant structure if the microwaves generated by a high-power gyrotron are efficiently coupled into the MAS stator through overmoded corrugated waveguides. We analyze the results and, based on experimental findings, suggest that significantly larger enhancements can be obtained at high field given the availability of sufficient microwave field strength.

II. THEORY

A. Diagonalization of the static Hamiltonian for the solid effect

The simplest system allowing us to describe the SE consists of two spins: an electron spin and a nuclear spin, with $S = I = \frac{1}{2}$. The static Hamiltonian describing this system contains the electron and nuclear Zeeman interaction between the respective spins and the external magnetic field as well as the electron-nuclear dipolar coupling between the two spins:

$$H_0 = \omega_{0S} S_z - \omega_{0I} I_z + A S_z I_z + B S_z I_x. \tag{1}$$

S_i and I_i are vector elements of the electron and nuclear spin operators $\vec{S}$ and $\vec{I}$, respectively, ω_{0S} and ω_{0I} denote the electron and nuclear Larmor frequencies, and A and B represent the secular and nonsecular part of the electron-nuclear dipolar coupling. Note that the following treatment is in accordance with that by Schweiger and Jeschke,[32] except for the sign of the nuclear Zeeman interaction, which we explicitly take as negative. Equation (1) is valid in the so-called "pseudo-high-field approximation" meaning all non-secular couplings are omitted, except those leading to a tilting of the nuclear eigenstates (BS_zI_x). Although Hu *et al.* recently published a detailed description of the diagonalization of this Hamiltonian,[33] we repeat some of the crucial steps in this section since they are important in the discussion of our experimental observations.

The Hamiltonian in (1) is block diagonal in the two-dimensional vector space $|S, m_S\rangle = |\frac{1}{2}, \pm\frac{1}{2}\rangle$ with the kets $|\alpha\rangle$ and $|\beta\rangle$ corresponding to $m_S = \pm 1/2$. As usual, the electron polarization operators are

$$S^{\alpha/\beta} = \frac{1}{2}\mathbf{E} \pm S_z, \tag{2}$$

where $\mathbf{E}$ is the unit operator. Inserting $S^{\alpha/\beta}$ leads to a new form of the Hamiltonian

$$H_0 = \omega_{0S} S_z \underbrace{-\omega_{0I} S^\alpha I_z + \frac{A}{2} S^\alpha I_z + \frac{B}{2} S^\alpha I_x}_{H_0^\alpha}$$
$$\underbrace{-\omega_{0I} S^\beta I_z - \frac{A}{2} S^\beta I_z - \frac{B}{2} S^\beta I_x}_{H_0^\beta} \tag{3}$$

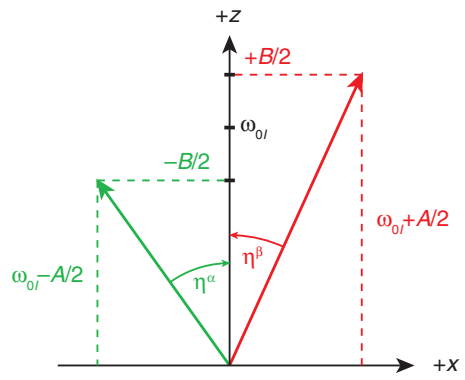

FIG. 1. Derivation of the branching angles in the α (green) and β (red) electron spin subspaces.

that can be easily diagonalized analytically by a unitary transformation

$$H_0^{\mathrm{D}} = U H_0 U^{-1} \tag{4}$$

with the transformation operator

$$U = e^{i\left(\eta^\alpha S^\alpha I_y + \eta^\beta S^\beta I_y\right)}. \tag{5}$$

The diagonalized Hamiltonian has the form:

$$H_0' = \omega_{0S} S_z - \omega^\alpha S^\alpha I_z - \omega^\beta S^\beta I_z \tag{6}$$

with

$$\omega^{\alpha,\beta} = \left(\omega_{0I} \mp \frac{A}{2}\right)\cos(\eta^{\alpha,\beta}) \pm \frac{B}{2}\sin(\eta^{\alpha,\beta}). \tag{7}$$

The branching angles are depicted in Fig. 1 and are defined as

$$\eta^{\alpha,\beta} = \arctan\left(\frac{B}{A \mp 2\omega_{0I}}\right) \text{ with } -\frac{\pi}{2} < \eta^{\alpha,\beta} < \frac{\pi}{2}. \tag{8}$$

Note that this definition of the $\eta^{\alpha,\beta}$ differs from the one used by Schweiger and Jeschke[32] since the second term in (1), $-\omega_{0I}I_z$, is negative rather than positive.

We satisfy the matching condition for the solid effect if the states connected by the zero or double quantum transitions are degenerate in the frame rotating with the frequency of the microwave irradiation ω_{mw}. In this case the matching condition is

$$\Delta\omega_{0S}^{(0,2)} = \mp\frac{\omega_{0I}}{2}(\cos\eta^\alpha + \cos\eta^\beta) \pm \frac{A}{4}(\cos\eta^\alpha - \cos\eta^\beta)$$
$$\mp\frac{B}{4}(\sin\eta^\alpha + \sin\eta^\beta), \tag{9}$$

where $\Delta\omega_{0S}^{(0)}$ and $\Delta\omega_{0S}^{(2)}$ are the microwave frequency offsets required for matching the zero and double quantum transition frequencies, respectively. We define $\Delta\omega_{0S}$ as

$$\Delta\omega_{0S} = \omega_{\mathrm{mw}} - \omega_{0S} \tag{10}$$

so that if $\Delta\omega_{0S} = \Delta\omega_{0S}^{(0)}$ or $\Delta\omega_{0S} = \Delta\omega_{0S}^{(2)}$, then the solid effect matching condition is satisfied.

In the case of $\omega_{0I} \gg \frac{A}{2}$ we see that the absolute values of the branching angles converge and we can define a common branching angle

$$\eta = \arctan\left(-\frac{B}{2\omega_{0I}}\right) \approx \eta^\alpha \approx -\eta^\beta. \tag{11}$$

In this limit Eq. (9) simplifies to the often-cited solid effect matching condition

$$\Delta\omega_{0S}^{(0,2)} = \pm\omega_{0I}. \tag{12}$$

Therefore, we satisfy the matching condition for the solid effect by irradiating the spin system at the sum or difference of the electron and nuclear Larmor frequencies.

B. Transition moments of the solid effect

In the limit of small microwave fields the transition moments for the double and zero quantum transitions can be obtained by transforming the rotating-frame microwave Hamiltonian

$$H_{\mathrm{mw}} = \omega_{1S} S_x \tag{13}$$

into the eigenframe of the static spin Hamiltonian H_0. We then obtain

$$H'_{\mathrm{mw}} = \omega_{1S}(S_x \cos\eta^- - 2S_y I_y \sin\eta^-) \tag{14}$$

with

$$\eta^- = \frac{\eta^\alpha - \eta^\beta}{2}. \tag{15}$$

H'_{mw} can be expressed on the basis of raising and lowering operators

$$\begin{aligned} S^\pm &= S_x \pm i S_y, \\ I^\pm &= I_x \pm i I_y, \end{aligned} \tag{16}$$

which yields

$$\begin{aligned} H'_{\mathrm{mw}} = \frac{\omega_{1S}}{2}\{&(S^+ + S^-)\cos\eta^- - [(S^+ I^- + S^- I^+) \\ &- (S^+ I^+ + S^- I^-)]\sin\eta^-\}. \end{aligned} \tag{17}$$

While the first term describes single quantum (SQ) EPR coherences, we see that introduction of an anisotropic electron-nuclear coupling with the non-secular component B, the second term becomes non-zero; therefore, zero and double quantum coherences can be generated which drive the solid effect transitions.

We make a further simplification by using the fact that $\omega_{0I} \gg A/2$. Using Eq. (11), we obtain

$$\begin{aligned} H'_{\mathrm{mw}} = \frac{\omega_{1S}}{2}\{&(S^+ + S^-)\cos\eta - [(S^+ I^- + S^- I^+) \\ &- (S^+ I^+ + S^- I^-)]\sin\eta\}. \end{aligned} \tag{18}$$

Simple trigonometric rules allow us to express Eq. (18) as

$$\begin{aligned} H'_{\mathrm{mw}} = \frac{\omega_{1S}}{2}\Bigg\{&\frac{2\omega_{0I}}{\sqrt{4\omega_{0I}^2 + B^2}}(S^+ + S^-) + \frac{B}{\sqrt{4\omega_{0I}^2 + B^2}} \\ &\times [(S^+ I^- + S^- I^+) - (S^+ I^+ + S^- I^-)]\Bigg\}. \end{aligned} \tag{19}$$

By further making the valid assumption of $\omega_{0I} \gg B/2$, we can simplify (19) to

$$\begin{aligned} H'_{\mathrm{mw}} = \frac{\omega_{1S}}{2}\Bigg\{&(S^+ + S^-) + \frac{B}{2\omega_{0I}}[(S^+ I^- + S^- I^+) \\ &- (S^+ I^+ + S^- I^-)]\Bigg\}. \end{aligned} \tag{20}$$

Equation (20) is derived for $\omega_{0I} \gg A, B$, and, since A and B decrease with increasing distance between the electron and the nuclear spins, it is only valid for nuclei which reside a certain radius from the electron spin. However, in a high magnetic field, this condition is satisfied for all protons of trityl and in the surrounding matrix.

In (20) we also see that the matrix elements driving the zero and double quantum solid effect transitions scale as $(\omega_{1S}B/\omega_{0I})$. So there are two possibilities to increase the transition moment at a given field for a given nucleus: (1) increase the microwave field strength $\omega_{1S,}$ or (2) increase the electron-nuclear coupling constant. (1) can be achieved by using higher power microwave sources and/or by improving the coupling of the microwave power to the sample volume and is therefore an engineering problem. (2) is an inherent characteristic of the sample itself. For a given nucleus the electron-nuclear dipolar coupling is modulated by the distance and orientation with respect to the external magnetic field vector. The orientation plays a crucial role since the non-secular component vanishes, if one of the principal axes of the electron-nuclear coupling tensor is parallel to the magnetic field vector.

C. DNP kinetics based on rate equations

All of the derivations in Secs. II A and II B describe the evolution of the state of a single electron-nucleus pair in the absence of any relaxation processes. However, SE DNP is a non-coherent transfer of electron polarization to nuclei, and therefore to describe the kinetics of polarization buildup in an ensemble of nuclei during a DNP experiment, it is essential to include the relaxation processes that govern the behavior of the system. In this section we derive the rate equations describing the polarization transfer. This approach, in combination with results obtained in Secs. II A and II B allows us to calculate a rate constant, k_{DNP}, which describes the initial DNP polarization transfer. This approach has been treated in detail by Smith *et al.*,[31] and the validity of this derivation has been discussed extensively. It was shown that this treatment is valid and applicable if changes in the observed nuclear polarization occur on a timescale slow compared to that of individual coherences, which typically occur on a timescale of a few milliseconds or shorter. We show in a subsequent section that the experimental buildup time constant is a few tens of seconds, so this assumption is valid for the case considered here.

Here we present the equations describing the excitation of the double quantum (DQ) electron-nuclear coherence. A similar treatment can be performed for the zero quantum (ZQ) case, which is shown in the supplementary material.[46] We begin with the complete electron-nuclear spin Hamiltonian including the microwave induced coupling terms in the eigenframe of the static Hamiltonian:

$$\begin{aligned} H' = \Delta\omega_{0S} S_z - \omega_{0I} I_z + A S_z I_z + \frac{\omega_{1S}}{2}(S^+ + S^-) \\ + \frac{\omega_{1S} B}{4\omega_{0I}}[(S^+ I^- + S^- I^+) - (S^+ I^+ + S^- I^-)]. \end{aligned} \tag{21}$$

Note that in (21) we neglected all shifts of population states due to state mixing. By using the sum and difference relations

$$S_z = \frac{1}{2}[(S_z + I_z) + (S_z - I_z)] \tag{22}$$

and

$$\Delta\omega_{0S} S_z - \omega_{0I} I_z = \frac{1}{2}[(\Delta\omega_{0S} - \omega_{0I})(S_z + I_z) + (\Delta\omega_{0S} + \omega_{0I})(S_z - I_z)], \tag{23}$$

we can express (21) as

$$\begin{aligned} H' = \frac{1}{2}\Bigg[& (\Delta\omega_{0S} - \omega_{0I})(S_z + I_z) \\ & + A(S_z + I_z)I_z - \frac{\omega_{1S}B}{2\omega_{0I}}(S^+I^+ + S^-I^-)\Bigg] \\ & + \frac{1}{2}\Bigg[(\Delta\omega_{0S} + \omega_{0I})(S_z - I_z) \\ & + A(S_z - I_z)I_z + \frac{\omega_{1S}B}{2\omega_{0I}}(S^+I^- + S^-I^+)\Bigg] \\ & + \frac{\omega_{1S}}{2}(S^+ + S^-). \end{aligned} \tag{24}$$

In (24) we see that all operators in the first summand correspond only to matrix elements in the DQ subspace in the full Hamiltonian, with elements represented in green in Fig. 2. Similarly, the second summand of Eq. (24) corresponds to the ZQ subspace (marked in red in Fig. 2). The third summand, at last, represents the SQ coherences between the electron-spin states (marked as blue in Fig. 2). By selecting the DQ matching condition for the solid effect (see Eq. (12)), we see that the two polarization states in the respective subframe become energetically degenerate (in the rotating frame), allowing for the appearance of DQ coherence between these states. We may neglect the ZQ coherence in this case, since we irradiate off-resonant by $2\omega_{0I}$, and the transition moment is small at the same time. Treatment of the SQ coherence term is more complicated: Due to the relatively large ratio between T_{1S} and T_{2S} in combination with the much larger SQ transition moment, electron spin polarization might be significantly reduced by off-resonant excitation of the EPR (SQ) transition despite being far off-resonance. However, by assuming that a quasi-equilibrium treatment is valid, we can mathematically uncouple the SQ and the DQ excitation without introducing significant errors, as long as transverse relaxation of the electron SQ coherence (described by T_{2S}) is fast compared to the DNP transfer. This allows us to easily describe an effectively reduced electron spin polarization and reduced electron T_{1S} by the well known steady-state solution of the Bloch equations,[34] and as detailed by Smith *et al.*[31] The DQ excitation can then be treated neglecting the SQ coherences, while the influence of the SQ coherence is represented by the reduced effective electron polarization and reduced electron T_1. The same arguments hold for the ZQ case; we only have to substitute DQ with ZQ and vice versa in the description above. However, we will only focus on the DQ treatment from now on.

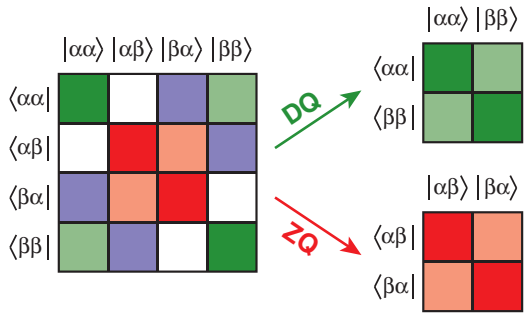

FIG. 2. The full Hamiltonian (left) in the eigenframe of the static Hamiltonian (see Eq. (21)) can be separated into the DQ (green) and the ZQ (red) subspaces, if the SQ coherences (light blue) are neglected. Coherence states are marked with light color, population states with dark color.

With the above conditions in mind, we can separate the DQ subspace from the full Hamiltonian:

$$\begin{aligned} H'_{\mathrm{DQ}} = \frac{1}{2}\Bigg[& \Omega^{\mathrm{DQ}}_{\mathrm{DNP}}(S_z + I_z) + A(S_z + I_z)I_z \\ & - \frac{\omega_{1S}B}{2\omega_{0I}}(S^+I^+ + S^-I^-)\Bigg]. \end{aligned} \tag{25}$$

In (25) we have introduced $\Omega^{\mathrm{DQ}}_{\mathrm{DNP}} = \Delta\omega_{0S} - \omega_{0I}$ as the offset between the microwave frequency and the DQ matching condition. Furthermore, we can drop the secular part of the electron-nuclear coupling term, since within this subspace the corresponding operator takes the form of an identity matrix and only leads to an offset of the eigenstates in the DQ subspace with respect to the ZQ subspace. We are left with a truncated DQ Hamiltonian of the form

$$H'^{(\mathrm{t})}_{\mathrm{DQ}} = \frac{1}{2}\left[\Omega^{\mathrm{DQ}}_{\mathrm{DNP}}(S_z + I_z) - \frac{\omega_{1S}B}{2\omega_{0I}}(S^+I^+ + S^-I^-)\right]. \tag{26}$$

If we consider this Hamiltonian in the DQ subspace (as depicted in Fig. 2), we see that it resembles a simple one-spin Hamiltonian consisting of a Zeeman term and a coupling term, driven by microwave irradiation. Accordingly, we can redefine a basis set for this subspace, which resembles the basis set of a single-spin in Hilbert-space. This basis set (including the respective raising and lowering operators) is given in Table I. We see that if the DQ matching condition is fulfilled, magnetization stored in $\langle S_z + I_z\rangle/2$ (corresponding to $\langle\sigma_z\rangle$ in the single spin case) is transformed into $\langle S^+I^+ - S^-I^-\rangle/2i$ (corresponding to $\langle\sigma_y\rangle$) under influence of the microwave term $(S^+I^+ + S^-I^-)/2$ (corresponding to σ_x). $\langle S^+I^+ - S^-I^-\rangle/2i$ magnetization will further evolve to $-\langle S_z + I_z\rangle/2$ and subsequently to $-\langle S^+I^+ - S^-I^-\rangle/2i$, and will finally return to $\langle S_z + I_z\rangle/2$. If the microwave frequency is applied with an offset to the actual DQ matching condition, magnetization in $\langle S^+I^+ - S^-I^-\rangle/2i$ will be in parallel evolving into $\langle S^+I^+ + S^-I^-\rangle/2$ and then into $-\langle S^+I^+ - S^-I^-\rangle/2i$, from where the microwave field will drive it back to $\langle S_z + I_z\rangle/2$; note that the return to $\langle S_z + I_z\rangle/2$ results in a reduction of the SE transfer efficiency. So we see that this spin system can be described by the common Bloch equations in analogy to a single spin system.

TABLE I. Spin-operators for a single spin (based on the Pauli spin operators σ_i) and the corresponding product spin operators for the electron-nuclear double quantum and zero quantum subspace as described in Eq. (24) and depicted in Fig. 2.

Single spin	Double quantum subspace	Zero quantum subspace
σ_z	$(S_z + I_z)/2$	$(S_z - I_z)/2$
σ_x	$S_xI_x - S_yI_y = (S^+I^+ + S^-I^-)/2$	$S_xI_x + S_yI_y = (S^+I^- + S^-I^+)/2$
σ_y	$S_yI_x + S_xI_y = (S^+I^+ - S^-I^-)/2i$	$S_yI_x - S_xI_y = (S^+I^- - S^-I^+)/2i$
$\sigma^+ = \sigma_x + i\sigma_y$	$S^+I^+ = S_xI_x - S_yI_y + i(S_yI_x + S_xI_y)$	$S^+I^- = S_xI_x + S_yI_y + i(S_yI_x - S_xI_y)$
$\sigma^- = \sigma_x - i\sigma_y$	$S^-I^- = S_xI_x - S_yI_y - i(S_yI_x + S_xI_y)$	$S^-I^+ = S_xI_x + S_yI_y - i(S_yI_x - S_xI_y)$

To do so, we define the following set of expectation values that fulfill the usual commutation relations:

$$\begin{aligned} P_S &= M_{S_z} = \langle S_z \rangle \\ P_I &= M_{I_z} = \langle I_z \rangle \\ M_x &= \langle S^+I^+ + S^-I^- \rangle/2 \\ M_y &= \langle S^+I^+ - S^-I^- \rangle/2i, \end{aligned} \tag{27}$$

where P_S and P_I are the polarization of the electrons and nuclear spins respectively, and M_x and M_y are the transverse DQ coherences.

We also define the effective transition moment for the solid effect transitions, according to Eq. (18):

$$\omega_{\mathrm{DNP}} = \omega_{1S} \sin \eta. \tag{28}$$

With these definitions at hand we formulate a set of Bloch-like differential equations describing the evolution of the spin system during solid effect DNP. For the sake of simplicity, we omit the effects caused by off-resonance excitation of the SQ EPR transition as well as the ZQ DNP transition. The former (i.e., the SQ excitation) can easily be solved with the usual Bloch equations, if line splitting due to secular electron-nuclear coupling is ignored. We will discuss the impact of this excitation later in the course of this paper.

First, we define a set of rate equations, describing the rate at which the expectation values introduced above change:

$$\begin{aligned} \frac{dP_S}{dt} &= -\omega_{\mathrm{DNP}} M_y + \frac{1}{T_{1S}}(P_{S,\mathrm{eq}} - P_S) \\ \frac{dP_I}{dt} &= \omega_{\mathrm{DNP}} M_y + \frac{1}{T_{1I}}(P_{I,\mathrm{eq}} - P_I) \\ \frac{dM_x}{dt} &= -\Omega_{\mathrm{DNP}} M_y - \frac{1}{T_{2,\mathrm{DNP}}} M_x \\ \frac{dM_y}{dt} &= \omega_{\mathrm{DNP}} \frac{(P_S - P_I)}{2} + \Omega_{\mathrm{DNP}} M_x - \frac{1}{T_{2,\mathrm{DNP}}} M_y. \end{aligned} \tag{29}$$

Note that the superscript of $\Omega_{\mathrm{DNP}}^{\mathrm{DQ}}$ has been dropped for simplicity. It is almost needless to mention that the ZQ case can similarly be described if several signs are inverted (a detailed derivation can be found in the supplementary material[46]).

We now assume that the coherences reach a quasi-steady state under microwave irradiation, which requires the timescale of the observation to be much slower than the evolution of the state, and therefore $dM_x/dt = dM_y/dt = 0$. Note that this does not prohibit changes in M_x and M_y in response to changes in P_S and P_I. Further, we define the rate constant

$$k_{\mathrm{DNP}} = \frac{\omega_{\mathrm{DNP}}^2 T_{2,\mathrm{DNP}}}{2(1 + (\Omega_{\mathrm{DNP}} T_{2,\mathrm{DNP}})^2)} \tag{30}$$

and assume that spin-diffusion leads to a fast equilibration of all nuclei. With the definition of the enhancement factor at infinite polarization time

$$\varepsilon_\infty = \frac{P_I^\infty}{P_{I,\mathrm{eq}}} \tag{31}$$

we find in the steady-state case

$$k_{\mathrm{DNP}} \left(\frac{P_S^\infty}{P_{I,\mathrm{eq}}} - \varepsilon_\infty \right) = \frac{1}{T_{1I}} (\varepsilon_\infty - 1). \tag{32}$$

This allows us to calculate our enhancement, if the DNP rate constant, the nuclear longitudinal relaxation time and the steady-state electron spin polarization are known:

$$\varepsilon_\infty = \frac{1 + k_{\mathrm{DNP}} T_{1I} \frac{P_S^\infty}{P_{I,\mathrm{eq}}}}{1 + k_{\mathrm{DNP}} T_{1I}} = \frac{1 + K_{\mathrm{DNP}} \frac{P_S^\infty}{P_{I,\mathrm{eq}}}}{1 + K_{\mathrm{DNP}}}. \tag{33}$$

Here, $K_{\mathrm{DNP}} = k_{\mathrm{DNP}} T_{1I}$ has been introduced, which can be considered as an effective DNP equilibrium constant between DNP buildup and polarization decay by longitudinal nuclear spin relaxation. If the steady-state enhancement and the steady-state electron polarization are known, K_{DNP} can be calculated by

$$K_{\mathrm{DNP}} = k_{\mathrm{DNP}} T_{1I} = \frac{(\varepsilon_\infty - 1)}{\left(\frac{P_S^\infty}{P_{I,\mathrm{eq}}} - \varepsilon_\infty \right)}. \tag{34}$$

III. EXPERIMENTAL

All experiments were performed using custom-built instrumentation including a MAS DNP spectrometer operating at 212 MHz ^{1}H frequency (courtesy of D. Ruben) and triple resonance (^{1}H, ^{13}C, ^{15}N) DNP probe. The probe is equipped with a sample eject system which allows continuous operation for several weeks at cryogenic temperatures and an arbitrary number of sample rotor ejections at temperatures of ~80 K.[35] 139.64 GHz (for simplicity, we will refer to this frequency as 140 GHz in the following) microwaves are generated with a gyrotron described elsewhere,[36] and transmitted to the MAS stator using an HE_{11} mode inside an overmoded, corrugated waveguide. The output power of the gyrotron was determined with a calorimeter immediately before the microwaves enter the DNP probe.

The NMR magnet is centered at 4.98 T and is equipped with a ±0.05 T superconducting sweep coil. The 140 GHz gyrotron is a fixed-frequency microwave source, and therefore a magnet with a superconducting sweep coil is required to set the field to the optimum position for polarizing agents with varying *g*-factors and/or different DNP mechanisms. Frequency-tunable gyrotrons are under development.[37]

The sample resides in a 4 mm outer diameter sapphire rotor with 0.7 mm wall thickness. Sapphire is the rotor material of choice because it is transparent at microwave frequencies. The sample is packed between Vespel spacers and has a height of ∼4 mm. All experiments were performed under 5 kHz MAS.

The polarizing agent is dissolved in the appropriate volume of a cryoprotecting mixture of d_8-glycerol/D_2O/H_2O (60:30:10 vol.-%) containing 1 M ^{13}C-urea. This glycerol/water ratio and the ^{1}H concentration of the matrix are known to provide optimum enhancements under most experimental DNP conditions. We dissolve trityl (OX063) in this solvent mixture to obtain a concentration of 40 mM; for comparison the Gd-DOTA is used at 10 mM. We also prepare samples with varying ^{1}H concentrations by dissolving an appropriate amount of polarizing agent together with ^{13}C-urea in pure d_8-, d_5-, or h_8-glycerol. This solution was then divided into equal parts and diluted with the required volumes of H_2O and D_2O to yield 60:40 vol.-% mixtures of glycerol/water with varying ^{1}H concentrations.

In all DNP experiments, the nuclear spin polarization was measured following a presaturation sequence and a period of polarization buildup. Presaturation on both ^{1}H and ^{13}C channels consisted of sixteen 108° pulses of 50 kHz rf strength (phase alternating along $+x$ and $+y$) separated by 5 ms. This was followed by a variable recovery time during which ^{1}H polarization is allowed to buildup. Polarization readout was performed via a ramped cross polarization (CP) step to ^{13}C for measurement of enhancement factors and buildup time constants, while for the measurement of the field dependent DNP enhancement profile ^{1}H polarization was directly measured via Bloch-decay. A CP spin-locking field of 83 kHz was applied on ^{1}H while the ^{13}C field was carefully optimized for highest CP efficiency. Under these conditions a contact time of 2 ms resulted in an optimal transfer of polarization from ^{1}H to ^{13}C for a sample of ^{13}C-urea in 60:30:10 vol.-% d_8-glycerol/D_2O/H_2O. This contact time was used for all experiments in this study. During acquisition of the FID an 83 kHz TPPM decoupling field was applied to ^{1}H.

The sample temperature was determined using a fiberoptical thermometer (Neoptix). The signal conditioner has been calibrated with the fiberoptical sensor being at room temperature and immersed in liquid nitrogen. In DNP experiments the sensor was attached to the outside of the stator housing. Therefore, all reported values represent the temperature of the stator housing and not of the actual sample.

IV. RESULTS AND DISCUSSION

A. Analysis of SE DNP matching conditions at 140 GHz

In order to locate the field that optimally satisfies the DNP matching condition, the ^{1}H DNP enhancement is recorded with a field sweep. The field sweep is centered around the trityl EPR resonance field at 4.982 T and spans a width that corresponds to at least twice the ^{1}H Larmor frequency of ∼212 MHz. The sweep width is chosen to cover both DNP transitions (i.e., the ZQ and the DQ transition), which includes broadening by inhomogeneity (e.g., *g*-anisotropy and electron-nuclear coupling). At each field position, the probe's ^{1}H channel was carefully retuned so that a constant level of reflected power was maintained throughout the total range of the field sweep and the intensity of the ^{1}H Bloch decay recorded. Off-signals (i.e., non-DNP enhanced signals) were observed at both field extrema of the sweep and show essentially no difference in intensity. This ensures that the sensitivity of the DNP probe does not change significantly across the field sweep that would otherwise lead to distortions in the field profile (Fig. 3). The ^{1}H field profile is normalized to unity, and, subsequently, the absolute ^{1}H DNP enhancement was determined via CP to ^{13}C at the field of maximum DNP enhancement to avoid significant ^{1}H background signals from probe components. This approach enables us to record high-quality, high-resolution field profiles in a relatively short period of time as illustrated by the data in Fig. 3.

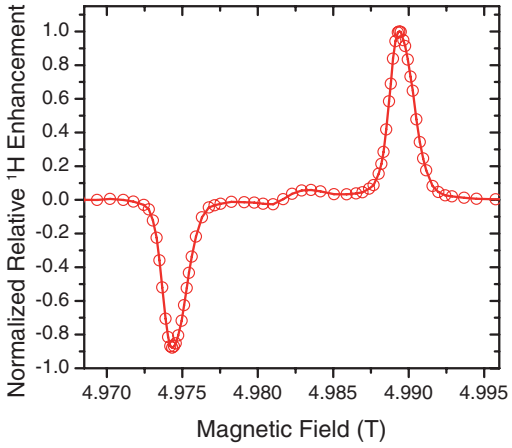

FIG. 3. 140 GHz DNP enhancement field profile for a 40 mM solution of trityl (OX063) in a mixture of 60:30:10 vol.-% d_8-glycerol/D_2O/H_2O recorded with a gyrotron microwave output power of 8 W at 85 K and 5 kHz MAS. Data points were obtained by recording the amplitude of the enhanced ^{1}H Bloch decay FID.

In Fig. 3 we show the field dependent enhancement profile obtained with 40 mM trityl (OX063), which exhibits two well-resolved peaks separated by a field equivalent to twice the ^{1}H Larmor frequency, clearly illustrating that solid effect is the dominant DNP mechanism. The shape of each DNP peak resembles the shape of the EPR spectrum since there is no significant overlap of positive and negative solid effect matching conditions. The maximum enhancement is observed by excitation of the DQ condition at the optimal field value of 4.9894 T. The ZQ transition at 4.9743 T yields a relative enhancement of −0.88 with respect to the maximum (positive) enhancement. Interestingly, DNP enhancements at fields corresponding to the allowed EPR transition are observed. These enhancements show a negative and a positive region, with a zero crossing close to the center of the EPR line. This is most probably caused by a low efficiency cross effect (CE) or

thermal mixing (TM). In a study by Borghini *et al.* similar observations were made using the BDPA radical at a field of 2.5 T and at temperatures as low as 0.7 K and explained as thermal mixing.[38]

The CE and TM require inhomogeneous or homogeneous broadening of the EPR line with an effective breadth matching at least the ^{1}H Larmor frequency (212 MHz). Although the inherent EPR line width (FWHM) of trityl is ∼50 MHz, there remains a small non-vanishing EPR amplitude covering a breadth of >212 MHz. The high concentration of 40 mM further allows for significant intermolecular electron-electron coupling required for the CE or TM. Maly *et al.* have shown that monomeric trityl radicals can be used as efficient polarizing agents for ^{2}H DNP at 5 T, and have therefore directly proven that the intermolecular electron-electron couplings between trityl molecules are sufficient for efficient CE.[39]

B. Polarization dynamics

Studies of the time dependence of the DNP enhancement as a function of microwave power performed at the field of maximum enhancement permit further analysis of the SE DNP mechanism. Buildup curves were acquired for three different microwave powers (3.3, 8.9, and 13.4 W). These results are compared to the respective data obtained without microwave irradiation, yielding the nuclear T_{1I} and off-signal amplitude. The buildup curves are displayed in Fig. 4, and the time constants are extracted from least-square fits with exponential functions. In the case of the non-DNP-enhanced signal (i.e. the "off-signal") it was necessary to utilize a biexponential function. The second component, which constitutes about 20% of the overall peak height, most likely arises from spins in the spacer material and consistently gives a $T_1 = 5.8$ s. Therefore, it can be easily distinguished from the slower buildup of ^{13}C-urea with $T_1 = 26.2$ s, and the DNP enhanced buildup curves were corrected for the background signal by subtracting this component before fitting with a monoexponential function. DNP enhancements were determined by dividing the amplitude of the infinite-time urea signal recorded with mw irradiation by that without mw irradiation. Results are listed in Table II.

TABLE II. Results of the analysis of 140 GHz DNP enhancements obtained with a 40 mM solution of trityl (OX063) in a mixture of 60:30:10 vol.-% d_8-glycerol/D_2O/H_2O. For definitions see Eqs. (37)–(39) below.

P_{mw} (W)	T (K)[a]	T_B (s)	ε_∞	k_{DNP}^{eff} (s^{-1})	$\frac{P_{S,eq}^{eff}}{P_{I,eq}}$	K_{DNP}^{eff}
0	82	26.2	1	0	660	0
3.26	85	24.9	26.6	2.03×10^{-3}	509	0.053
8.90	88	22.8	64.2	5.71×10^{-3}	486	0.150
13.41	92	21.0	90.6	9.39×10^{-3}	454	0.246

[a]Note that reported temperature values represent the temperature of the stator housing and not the sample itself.

As can be seen in Fig. 5, enhancements clearly show a near-linear behavior as function of incident microwave power. This is expected since in the theory above k_{DNP} scales with ω_{1S}^2, and ω_{1S}^2 scales linearly with microwave power. A slight deviation from linearity is seen, however, leading to a slight decrease in slope with higher microwave power. The buildup time constants are reduced compared to the spin-lattice relaxation constant under microwave irradiation and show a monotonic trend of faster buildup with higher microwave power.

Although we believe the reduced buildup times are a result of an increase in k_{DNP}, it is requisite to show that this reduction is not caused by sample heating due to microwave absorption in the sample rotor and/or the surrounding environment. Unfortunately, the determination of the actual sample temperature during MAS is not trivial. Mieville *et al.* have introduced a method to measure the sample temperature *in situ* by inserting a sample of KBr inside the rotor which then allows to indirectly determine the temperature by measuring the chemical shift or T_{1I} of ^{79}Br.[40] However, this approach has not been applied in our experiments. Instead, the stator temperature is measured as described in the Experimental section. High-frequency structure simulation (HFSS) studies have shown that only a small amount of the microwave power is actually dispersed inside the sample;[41] however, the sample temperature might still be affected indirectly due to heating of the surrounding stator. To determine if sample heating by microwave absorption plays a significant role in the polarization dynamics, we performed experiments at a magnetic

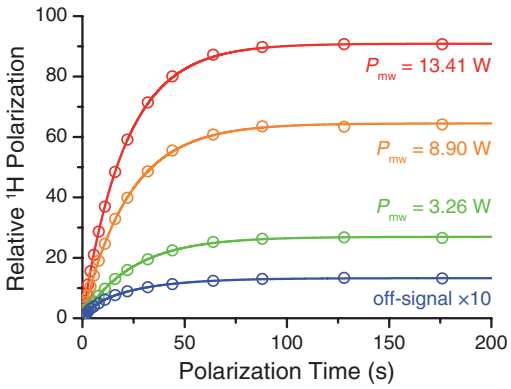

FIG. 4. 140 GHz DNP buildup curves for a 40 mM solution of trityl (OX063) in a mixture of 60:30:10 vol.-% d_8-glycerol/D_2O/H_2O recorded at various microwave power levels. For details see text and Table II.

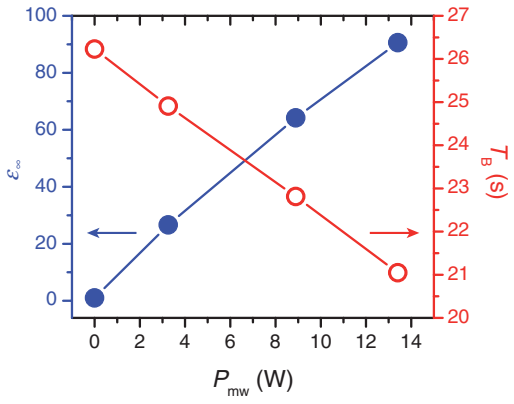

FIG. 5. Obtained 140 GHz DNP enhancements (filled blue circles) and buildup time constants (open red circles) for a 40 mM solution of trityl (OX063) in a mixture of 60:30:10 vol.-% d_8-glycerol/D_2O/H_2O recorded at various microwave power levels. For details see text and Table II.

TABLE III. Comparison of nuclear spin relaxation time T_{1I} at different field positions with and without microwave irradiation.

$\frac{\Omega_{0S}}{2\pi}$ (MHz)	P_{mw} (W)	T_1 (s)	T (K)[a]
−212.426	0	26.2	82
−1014.287	0	26.8	84
−1014.287	8.90	27.1	89

[a]Note that reported temperature values represent the temperature of the stator housing and not the sample itself.

field at which no DNP enhancement is obtained and compare T_{1I} with and without microwave irradiation. We chose a magnetic field equivalent to a frequency offset of $\Omega_{0S}/2\pi = -1014.3$ MHz with respect to the EPR transition. This offset ensures that no DNP enhancement is obtained. Relaxation time measurements were performed using 8.90 W of microwave power and compared to measurements without microwave power. The observed relaxation time constants are given in Table III. No significant difference can be observed when the probe and sample are subject to microwave irradiation, leading to the conclusion that sample heating is not a major issue and can furthermore be assumed as negligible under our experimental conditions since there is a reduction of T_{1I} expected with increasing temperature. Thus, the observed reduction of the polarization buildup time constants is safely ascribed to the polarization transfer mechanism.

A deviation of the observed enhancements as function of incident microwave power from linear behavior is expected, since significant polarization buildup in the ^{1}H bulk reduces the polarization gradient between electron spins and nuclear spins and therefore also reduces the effective DNP rate. At this point we remind the reader of the theoretical maximum enhancement factor of 660 for DNP of ^{1}H. This behavior can be better understood by further investigation of Eq. (33). In the limit of large K_{DNP}, the enhancement approaches $P_S^\infty / P_{I,eq}$. Assuming the electron spin preserves its thermal equilibrium polarization due to fast relaxation, we achieve the maximum enhancement given by γ_S/γ_I. However, if the electron spin polarization is depleted from its thermal equilibrium during DNP and has a lower steady-state polarization, the maximum enhancement that can be obtained will be below that ratio.

With our present instrumentation, we have no knowledge of the electron spin steady-state polarization during DNP or K_{DNP}. Therefore, we cannot directly utilize (34) to calculate K_{DNP} from the measured value of ε_∞ or vice versa. However, we can estimate the steady-state electron polarization based on a model we have proposed recently.[31] This model describes the polarization transfer between electron spin and nuclear spins that was observed for static (i.e., non-MAS) DNP experiments using the same polarizing agent (i.e., trityl) inside a microwave cavity. In this model the nuclear spins are divided into nearby and distant (i.e., bulk) spins, which are spatially separated by the spin-diffusion barrier. During DNP, the electron spin transfers polarization to these nearby and distant nuclei baths in parallel. Spins within the volume confined by the spin-diffusion barrier experience fast, paramagnetically enhanced spin-lattice relaxation and are not able to transfer the polarization to more distant nuclei before it relaxes to the lattice. DNP transfer to more distant spins which are situated outside of the spin-diffusion barrier is most likely slower due to reduced dipolar coupling (scaling with r^{-3}); at the same time paramagnetic relaxation is strongly attenuated since its effects scale as r^{-6}. This allows the polarization transferred to these distant spins to efficiently disperse the enhanced polarization throughout the bulk. In other words, a significant amount of electron spin polarization is "drained" from the electron spin by fast-relaxing nuclei in the close proximity of the electron spin, whereas polarization transferred directly to spins more distant to the electron leads to the observable DNP enhancement.

Another mechanism of electron spin polarization depletion is off-resonant excitation of the EPR transition which can be described by evoking one solution of the Bloch equations:

$$P^*_{S,eq} = P_{S,eq}\frac{1+\Omega_{0S}^2 T_{2S}^2}{1+\Omega_{0S}^2 T_{2S}^2+\omega_{1S}^2 T_{1S} T_{2S}}. \tag{35}$$

Ω_{0S} is the resonance offset between the excitation frequency and the electron spin Larmor frequency and in our case is $\Omega_{0S}/2\pi = \omega_{0I}/2\pi = 212.428$ MHz which is the solid effect matching condition. Although we have experimentally determined relaxation times $T_{1S} = 1.43$ ms and $T_{2S} = 0.89$ μs for trityl at 80 K as described previously,[31] we do not know the conversion factor, c, between the incident microwave power and the oscillating microwave field amplitude B_1

$$c = \frac{\gamma_S B_{1S}}{2\pi\sqrt{P_{mw}}} = \frac{\omega_{1S}}{2\pi\sqrt{P_{mw}}}. \tag{36}$$

This prevents us from distinguishing between polarization depletion by off-resonant excitation and by DNP transfer to fast-relaxing nuclei. Nanni *et al.* have estimated the microwave field distribution inside a MAS stator used for 250 GHz DNP, and arrived at an average conversion factor of 0.31 MHz W$^{-0.5}$ for an experimental arrangement similar to that used here.[41] Assuming the same conversion factor in our experiments leads us to an average value of $\omega_{1S}/2\pi = 1.15$ MHz for the highest applied microwave power of 13.41 W. This field strength would lead to a depletion of ~4% which can be considered as negligible. Increasing the field strength to 2 or 3 MHz, however, would lead to 12% and 24% depletion, respectively.

The remaining electron spin polarization − which is available for transfer to distant nuclei − can be approximated by knowledge of the longitudinal nuclear spin relaxation time constant, DNP buildup time constant as well as the obtained enhancement. Due to the fact that the buildup of the longitudinal nuclear spin polarization is accelerated by the solid effect (as can be seen in Fig. 5) an effective DNP rate constant can be obtained from the observed buildup time constant T_B and by the nuclear spin-lattice relaxation time constant T_{1I}. This effective DNP rate constant is given by

$$k_{DNP}^{eff} = \frac{1}{T_B} - \frac{1}{T_{1I}}. \tag{37}$$

Assuming that the polarization builds up equally fast on all bulk nuclear spins (i.e., ^{1}H−^{1}H spin diffusion is fast compared to the DNP transfer rate) we can calculate the effective

electron spin polarization by

$$\frac{P^{\text{eff}}_{S,\text{eq}}}{P_{I,\text{eq}}} = \frac{1}{k^{\text{eff}}_{\text{DNP}}}\left(\frac{\varepsilon_\infty}{T_\text{B}} - \frac{1}{T_{1I}}\right). \tag{38}$$

This depleted steady-state polarization includes polarization loss by transfer to nearby spins (which drain the polarization by fast paramagnetically enhanced longitudinal relaxation) as well as saturation due to off-resonant excitation as described earlier. The reader should note that $P^{\text{eff}}_{S,\text{eq}}$ describes the effective electron spin polarization and replaces the thermal equilibrium polarization. P^{∞}_{S}, on the other hand, denotes the steady-state polarization during the DNP of bulk nuclei; so $P^{\text{eff}}_{S,\text{eq}}$ and P^{∞}_{S} are not generally equal. However, under the assumption that DNP to distant nuclei does not significantly deplete the electron spin polarization, we can use the condition $P^{\infty}_{S} = P^{\text{eff}}_{S,\text{eq}}$ in Eq. (34) in order to calculate $K^{\text{eff}}_{\text{DNP}}$:

$$K^{\text{eff}}_{\text{DNP}} = \frac{(\varepsilon^{\infty} - 1)}{\left(\frac{P^{\text{eff}}_{S,\text{eq}}}{P_{I,\text{eq}}} - \varepsilon^{\infty}\right)}. \tag{39}$$

Because of the low conversion factor between P_{mw} and ω_{1S} as well the low effective ω_{DNP}, due to operation in high magnetic field, this assumption seems to be safe. However the large ratio between nuclear spins and electron spins still might lead to a significant depletion of electron spin polarization.

This set of equations now allow us to calculate the effective DNP rate constant, the electron spin polarization available for DNP buildup on distant (bulk) nuclei as well as validate the theoretically proposed linearity between $K^{\text{eff}}_{\text{DNP}}$ as a measure of the solid effect efficiency and the incident microwave power. A detailed analysis of the experimental data is presented in Table II and depicted in Fig. 6. We clearly see that $K^{\text{eff}}_{\text{DNP}}$ is nearly linear with the microwave power, as expected; however, to calculate $K^{\text{eff}}_{\text{DNP}}$ from experiments, we assumed that $P^{\infty}_{S} = P^{\text{eff}}_{S,\text{eq}}$. If this assumption failed, then the calculated $K^{\text{eff}}_{\text{DNP}}$ would diverge from linearity. The validity of this assumption suggests that the transfer of polarization from the electron to distant nuclei only has a minor effect on the final electron polarization, P^{∞}_{S}. However, Fig. 6 shows that the effective electron spin polarization, $P^{\text{eff}}_{S,\text{eq}} / P_{I,\text{eq}}$, does change significantly during DNP. The effective electron spin polarization undergoes a fast reduction at rather low microwave powers and a rather small negative slope towards higher incident power. This might be explained by a fast "saturation" (i.e., equilibration of electron and nuclear spin polarization) of the nearby nuclei that cannot efficiently spread their polarization to the bulk due to hindered spin-diffusion through the barrier.

C. Influence of spin-diffusion efficiency on DNP

In order to investigate the role of homonuclear spin-diffusion in SE DNP, we prepared samples with a constant concentration of the polarizing agent, but with varying ^{1}H concentrations. We varied the ^{1}H concentration by choosing the appropriate ratio between D_2O and H_2O in the matrix or by substituting perdeuterated glycerol (d_8) with partially deuterated (d_5) or fully protonated glycerol. Here we note that

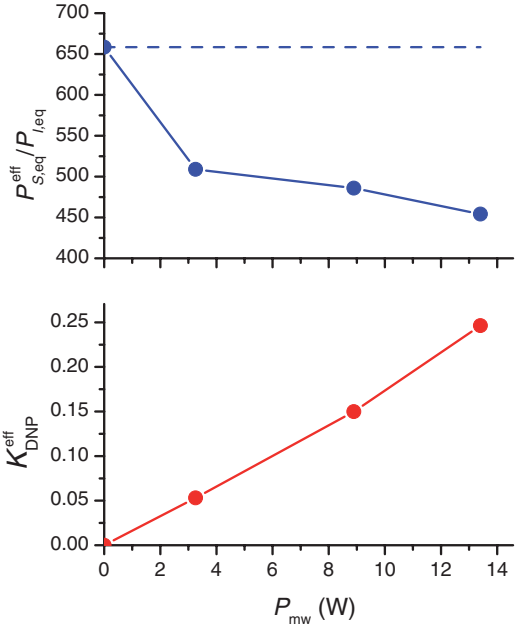

FIG. 6. Top: calculated $P^{\text{eff}}_{S,\text{eq}} / P_{I,\text{eq}}$ according to Eq. (38) for various incident microwave power levels. The dashed line represents the maximum value of 660. Bottom: $K^{\text{eff}}_{\text{DNP}}$ according to Eq. (39) as function of microwave power. For details see text and Table II.

a 2 ms CP contact time was used for all samples. We expect variations in CP efficiency for different protonation levels, which are shown in Fig. 7 (bottom) where we plot the off-signal amplitude. However, the buildup times and enhancements for a given sample do not depend on CP efficiency; these parameters only depend on measurement of relative signal intensity within the set of experiments on one sample. We also note that even in the worst case, the signal amplitude could only be increased by a maximum of ~25% by shortening of the contact time.

In Fig. 7 (top) the enhancements obtained with 40 mM trityl are shown in comparison to experiments using 10 mM Gd-DOTA as polarizing agent. Trityl achieves the largest enhancement at minimum ^{1}H concentration and the enhancement drops monotonically if more protons are available. Gd-DOTA shows the opposite behavior with increasing enhancements for higher ^{1}H concentration, and reaches a plateau value of ~12 above ~20 M ^{1}H. Furthermore, in the case of trityl, the increase of ^{1}H concentration has only a limited influence on the buildup time constants. The buildup time constants are practically invariant at low ^{1}H concentrations (with a constant value of ~25 s) and only show a slight reduction of 30%-40% above 25 M ^{1}H (see Fig. 7, middle). When using Gd-DOTA as a polarizing agent, the buildup kinetics show a very rapid decrease of the buildup time constant if the ^{1}H concentration is increased from the minimum concentration. For a fully protonated matrix we observed a more than 4-fold reduction in buildup time constants. The combination of higher enhancement and shorter buildup time constant with higher ^{1}H concentration renders the use of deuterated solvents unnecessary and even detrimental in the case of Gd-DOTA.

This overall behavior indicates that the solid effect is active in two different limits when comparing the different

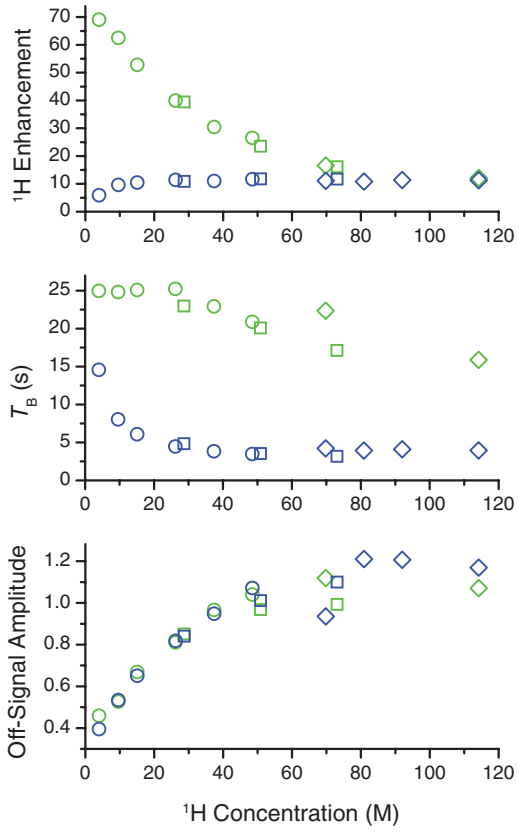

FIG. 7. Comparison of DNP parameters between the polarizing agents trityl (OX063) (green) and Gd-DOTA (blue) for various ^{1}H concentrations in the matrix. Top: enhancement factors, obtained by comparing on- and off-signal amplitude after a polarization time of 1.26 times T_B; middle: buildup time constants; bottom: non-DNP-enhanced off-signal amplitudes after a recovery time of 1.26 times T_B. Open circles represent samples prepared with d_8-glycerol, whereas open squares and diamonds correspond to samples prepared with d_5- and h_8-glycerol, respectively. The glycerol/water ratio was 60/40 (v/v) in all cases, with 40 mM polarizing agent concentration for trityl and 10 mM in case of Gd-DOTA. All data points were recorded under 8 W microwave power at a temperature of ~86 K.

polarizing agents. When using trityl, the kinetics during the DNP process are dominated by a rate-limiting step which involves a relatively slow initial polarization transfer from the electron spin to the nuclear spins; Gd-DOTA on the other hand is limited by a relatively inefficient spin-diffusion whereas the initial polarization step is not rate-limiting. We propose two causes for these differences: (1) The polarization of the $S = 1/2$ electron spin in trityl relaxes much slower than in the case of the $S = 7/2$ high-spin Gd(III). This causes a significant depletion of the electron spin polarization of trityl, leading to a smaller polarization gradient between electron spin and nuclear spins and therefore lower enhancements if a greater number of nuclear spins are to be polarized due to higher concentration of protons. Gd(III) might not be limited by this effect because T_{1S} is several orders of magnitude shorter. (2) The high-spin state of Gd-DOTA induces a transition moment that is four times higher for all coherences involving transitions between the $m_S = -1/2$ and $m_S = +1/2$ states, including the solid effect transitions involved in DNP. This leads to a higher efficiency of the initial polarization transfer. At the same time, the $S = 7/2$ spin induces much stronger paramagnetic relaxation and shifts of the surrounding nuclei which result in a larger ratio of nearby to distant (i.e., bulk) nuclei. This renders a greater fraction of the protons undetectable due to paramagnetic shifts, fast relaxation, and impeded spin-diffusion from those spins to the bulk. This can be seen if one compares the off-signal amplitudes between samples doped with trityl and those doped with Gd-DOTA. In Fig. 7 (bottom) we see that both 40 mM trityl and 10 mM Gd-DOTA have similar off-signal amplitudes, although the concentration of trityl is 4-fold higher. This indicates that the volume of exclusion per electron spin due to paramagnetic effects is four times larger in the case of Gd-DOTA compared to trityl.

In conclusion, the concentration dependence of the buildup dynamics using Gd-DOTA *vs*. trityl suggest that solid effect enhancements obtained with Gd-DOTA are limited by spin-diffusion, whereas the initial polarization transfer rate limits the solid effect enhancements for trityl; this may be due to a higher DNP transition moment and stronger paramagnetic effects for Gd-DOTA as compared to trityl.

D. The solid effect at fields > 5 T

In light of the improvement in SE enhancements reported here and since higher magnetic fields are generally of more interest to the NMR community, it is important to consider the extent to which the solid effect can be used at $B_0 > 5$ T. The experimental findings in the preceding sections strongly indicate that the SE is currently limited by the available microwave field strength. Furthermore, the solid effect enhancements scale as B_0^{-2},[16–18] due to the attenuation of state mixing at higher magnetic field. In Eq. (20) one can see that this field dependence can be compensated if the microwave field strength scales linearly with B_0. Concurrently, for a fixed conversion factor, the microwave field scales as the square root of the power potentially leading to arcing and sample heating. Enhancing the conversion factor between incident microwave power and field generated by introduction of a resonant structure with a small MAS rotor might solve this problem.[42,43] This approach could be used with microwave frequencies in the range between 100 and 300 GHz, but for higher frequencies the dimensions of the resonator would drop below 1 mm, at which point fabrication becomes a challenge. A Fabry-Perot resonator design might be beneficial at frequencies >300 GHz, however, avoiding coupling between the standing microwave field and the rf pickup device would be challenging.

A second possible problem associated with very high microwave fields might be the off-resonant excitation of the single quantum EPR line. Earlier we have indicated that saturation of the single quantum transition does not play a significant role for the power levels used in this study and will not be a major issue even for microwave fields that are ~2–3 times larger. When transitioning to higher fields, the microwave field amplitude has to be scaled linearly with the external magnetic field to maintain a constant transition moment; on its own, the increase in microwave field would worsen off-resonant saturation. However, we note that the frequency offset must also be scaled linearly with the external

magnetic field to meet the SE matching condition. Therefore, the required increases in microwave field amplitude and microwave frequency offset are proportional. By analyzing Eq. (35) and assuming a constant ratio between nuclear Larmor frequency and microwave field (i.e., $\omega_{1S} = b\omega_{0I}$), as well as field independent relaxation time constants, we see that

$$\lim_{\omega_{0I}\to\infty}\left(P_{S,\mathrm{eq}}\frac{1+\omega_{0I}^2T_{2S}^2}{1+\omega_{0I}^2T_{2S}^2+b^2\omega_{0I}^2T_{1S}T_{2S}}\right)=\frac{P_{S,\mathrm{eq}}T_{2S}}{T_{2S}+b^2T_{1S}}. \tag{40}$$

The polarization depletion by off-resonant irradiation converges to a constant value if the frequency offset and the microwave field amplitude are scaled the same way as the external magnetic field (in the case that the inhomogeneous linewidth is much smaller than the nuclear Larmor frequency). Therefore we predict that off-resonant saturation of the single quantum transition will not be of major concern at higher fields.

A final concern is the small but non-vanishing *g*-anisotropy of polarizing agents such as trityl or BDPA. Whereas the g-anisotropy is barely visible at 5 T, it will lead to a considerable broadening at higher magnetic fields and a reduction of the solid effect efficiency. Recently we have introduced high-spin paramagnetic complexes based on Gd(III) and Mn(II).[44] Since these complexes show no spin-orbit coupling, they feature a nearly isotropic electron Zeeman interaction. However, the central $m_S = -1/2 \rightarrow +1/2$ transition is broadened by a significant second-order zero-field splitting (i.e., electron quadrupole interaction), which manifests itself in a 29 MHz full width at half maximum (FWHM) in the case of Gd-DOTA at 5 T, for example. ^{1}H solid effect enhancements of ∼20 have been obtained with this polarizing agent under the same experimental conditions used in this study. The line broadening second-order effect, however, is expected to decrease linearly with ω_0.[45] This makes Gd-DOTA a potential candidate as a polarizing agent for the solid effect at fields >5 T, since the broadening disadvantage of trityl with increasing field is substituted by a narrowing advantage of Gd-DOTA.

The combination of all these facts suggests that significant enhancements could be reached with the solid effect even at magnetic fields >5 T. However, this requires that high microwave power is available at the respective frequencies, which may be technically very challenging.

V. CONCLUSION

We have shown that significant enhancements of ∼91 are observed with the solid effect using trityl (OX063) as polarizing agent at a magnetic field of 5 T in MAS DNP. The enhancement factors and polarization buildup dynamics have been recorded for three different microwave power levels. The enhancements are currently limited by the available microwave power and could likely be increased if higher power becomes available. An analysis of the experimental data suggests good agreement with the theoretical model proposed by Smith *et al.*,[31] which was developed using data recorded under static (non-MAS) NMR conditions. The two data sets show no significant mechanistic differences which leads us to conclude that both the initial DNP step of polarization transfer from the electron spin to the nuclei as well as the further spreading of polarization within the nuclear spin bath contribute similarly to the overall DNP process.

We investigated the role of homonuclear spin-diffusion in solid effect DNP by varying the ^{1}H concentration of the sample using trityl and compared the results to those obtained with the polarizing agent Gd-DOTA. Differences observed between the two polarizing agents most probably arise because the solid effect is operating in two different kinetic regimes: In the case of trityl the initial polarization transfer step between the electron spin and the bulk nuclear spin bath is relatively slow and rate-limiting, whereas the subsequent ^{1}H–^{1}H spin-diffusion is fast. For Gd-DOTA the opposite is the case. While the initial polarization step is fast, the dispersion of polarization to the bulk protons is rate-limiting. Possible reasons for this fundamental difference can be found in drastically different electron spin relaxation properties of trityl and Gd-DOTA, a higher ZQ and DQ transition moment due to the high-spin properties of Gd(III) as well as in differences in paramagnetic relaxation and shifts of nuclear spins induced by the high-spin state.

We further discussed possible problems and advantages of the solid effect at fields >5 T. We predict that the solid effect will be a viable experiment at higher magnetic fields, if sufficient microwave power is available at the required frequencies.

ACKNOWLEDGMENTS

The authors thank Loren B. Andreas and Alexander B. Barnes for helpful discussions. Special thanks are accorded to I. Bertini and C. Luchinat for suggesting experiments with Gd-DOTA. Financial support was provided by NIH Grant Nos. EB002804 and EB002026. B.C. was partially supported by a DFG research fellowship (Grant No. CO802/1-1).

[1] A. W. Overhauser, Phys. Rev. **92**(2), 411–415 (1953).
[2] T. R. Carver and C. P. Slichter, Phys. Rev. **92**(1), 212–213 (1953).
[3] M. Abraham, R. W. Kedzie, and C. D. Jeffries, Phys. Rev. **106**(1), 165–166 (1957).
[4] A. Abragam and W. G. Proctor, C. R. Hebd. Seances Acad. Sci. **246**(15), 2253–2256 (1958).
[5] C. D. Jeffries, Phys. Rev. **117**(4), 1056–1069 (1960).
[6] A. V. Kessenikh, V. I. Lushchikov, A. A. Manenkov, and Y. V. Taran, Sov. Phys. Solid State **5**(2), 321–329 (1963).
[7] C. F. Hwang and D. A. Hill, Phys. Rev. Lett. **18**(4), 110–112 (1967).
[8] C. F. Hwang and D. A. Hill, Phys. Rev. Lett. **19**(18), 1011–1014 (1967).
[9] D. S. Wollan, Phys. Rev. B **13**(9), 3671–3685 (1976).
[10] D. S. Wollan, Phys. Rev. B **13**(9), 3686–3696 (1976).
[11] M. Goldman, *Spin Temperature and Nuclear Magnetic Resonance in Solids* (Oxford University Press, London, 1970).
[12] A. Abragam and M. Goldman, Rep. Prog. Phys. **41**(3), 395–467 (1978).
[13] W. T. Wenckebach, Appl. Magn. Reson. **34**(3-4), 227–235 (2008).
[14] J. H. Ardenkjær-Larsen, I. Laursen, I. Leunbach, G. Ehnholm, L. G. Wistrand, J. S. Petersson, and K. Golman, J. Magn. Reson. **133**(1), 1–12 (1998).
[15] C. F. Koelsch, J. Am. Chem. Soc. **79**(16), 4439–4441 (1957).
[16] T. Maly, G. T. Debelouchina, V. S. Bajaj, K. N. Hu, C. G. Joo, M. L. Mak-Jurkauskas, J. R. Sirigiri, P. C. A. van der Wel, J. Herzfeld, R. J. Temkin, and R. G. Griffin, J. Chem. Phys. **128**(5), 052211 (2008).
[17] A. B. Barnes, G. De Paepe, P. C. A. van der Wel, K. N. Hu, C. G. Joo, V. S. Bajaj, M. L. Mak-Jurkauskas, J. R. Sirigiri, J. Herzfeld, R. J. Temkin, and R. G. Griffin, Appl. Magn. Reson. **34**(3-4), 237–263 (2008).

[18]R. G. Griffin and T. F. Prisner, Phys. Chem. Chem. Phys. **12**(22), 5737–5740 (2010).
[19]K. N. Hu, V. S. Bajaj, M. Rosay, and R. G. Griffin, J. Chem. Phys. **126**(4), 044512 (2007).
[20]K. N. Hu, H. H. Yu, T. M. Swager, and R. G. Griffin, J. Am. Chem. Soc. **126**(35), 10844–10845 (2004).
[21]C. Song, K.-N. Hu, C.-G. Joo, T. M. Swager, and R. G. Griffin, J. Am. Chem. Soc. **128**(35), 11385–11390 (2006).
[22]K. N. Hu, C. Song, H. H. Yu, T. M. Swager, and R. G. Griffin, J. Chem. Phys. **128**(5), 052302 (2008).
[23]Y. Matsuki, T. Maly, O. Ouari, H. Karoui, F. Le Moigne, E. Rizzato, S. Lyubenova, J. Herzfeld, T. Prisner, P. Tordo, and R. G. Griffin, Angew. Chem., Int. Ed. **48**(27), 4996–5000 (2009).
[24]A. B. Barnes, B. Corzilius, M. L. Mak-Jurkauskas, L. B. Andreas, V. S. Bajaj, Y. Matsuki, M. L. Belenky, J. Lugtenburg, J. R. Sirigiri, R. J. Temkin, J. Herzfeld, and R. G. Griffin, Phys. Chem. Chem. Phys. **12**(22), 5861–5867 (2010).
[25]K. R. Thurber, W. M. Yau, and R. Tycko, J. Magn. Reson. **204**(2), 303–313 (2010).
[26]E. L. Dane, B. Corzilius, E. Rizzato, P. Stocker, T. Maly, A. A. Smith, R. G. Griffin, O. Ouari, P. Tordo, and T. M. Swager, J. Org. Chem. **77**(4), 1789–1797 (2012).
[27]M. K. Kiesewetter, B. Corzilius, A. A. Smith, R. G. Griffin, and T. M. Swager, J. Am. Chem. Soc. **134**(10), 4537–4540 (2012).
[28]Y. Hovav, A. Feintuch, and S. Vega, J. Magn. Reson. **207**(2), 176–189 (2010).
[29]A. Feintuch, D. Shimon, Y. Hovav, D. Banerjee, I. Kaminker, Y. Lipkin, K. Zibzener, B. Epel, S. Vega, and D. Goldfarb, J. Magn. Reson. **209**(2), 136–141 (2011).
[30]Y. Hovav, A. Feintuch, and S. Vega, J. Chem. Phys. **134**(7), 074509 (2011).
[31]A. A. Smith, B. Corzilius, A. B. Barnes, T. Maly, and R. G. Griffin, J. Chem. Phys. **136**(1), 015101 (2012).
[32]A. Schweiger and G. Jeschke, *Principles of Pulse Electron Paramagnetic Resonance*, 1st ed. (Oxford University Press, Oxford, 2001).
[33]K. N. Hu, G. T. Debelouchina, A. A. Smith, and R. G. Griffin, J. Chem. Phys. **134**(12), 125105 (2011).
[34]F. Bloch, W. W. Hansen, and M. Packard, Phys. Rev. **69**(11-1), 680–680 (1946).
[35]A. B. Barnes, M. L. Mak-Jurkauskas, Y. Matsuki, V. S. Bajaj, P. C. A. van der Wel, R. DeRocher, J. Bryant, J. R. Sirigiri, R. J. Temkin, J. Lugtenburg, J. Herzfeld, and R. G. Griffin, J. Magn. Reson. **198**(2), 261–270 (2009).
[36]L. R. Becerra, G. J. Gerfen, R. J. Temkin, D. J. Singel, and R. G. Griffin, Phys. Rev. Lett. **71**(21), 3561–3564 (1993).
[37]A. C. Torrezan, S. T. Han, I. Mastovsky, M. A. Shapiro, J. R. Sirigiri, R. J. Temkin, A. B. Barnes, and R. G. Griffin, IEEE Trans. Plasma Sci. **38**(6), 1150–1159 (2010).
[38]M. Borghini, W. de Boer, and K. Morimoto, Phys. Lett. A **48**(4), 244–246 (1974).
[39]T. Maly, L. B. Andreas, A. A. Smith, and R. G. Griffin, Phys. Chem. Chem. Phys. **12**(22), 5872–5878 (2010).
[40]P. Miéville, V. Vitzthum, M. A. Caporini, S. Jannin, S. Gerber-Lemaire, and G. Bodenhausen, Magn. Reson. Chem. **49**(11), 689–692 (2011).
[41]E. A. Nanni, A. B. Barnes, Y. Matsuki, P. P. Woskov, B. Corzilius, R. G. Griffin, and R. J. Temkin, J. Magn. Reson. **210**(1), 16–23 (2011).
[42]A. Brinkmann, S. K. Vasa, H. Janssen, and A. P. M. Kentgens, Chem. Phys. Lett. **485**(4-6), 275–280 (2010).
[43]V. Weis, M. Bennati, M. Rosay, J. A. Bryant, and R. G. Griffin, J. Magn. Reson. **140**(1), 293–299 (1999).
[44]B. Corzilius, A. A. Smith, A. B. Barnes, C. Luchinat, I. Bertini, and R. G. Griffin, J. Am. Chem. Soc. **133**(15), 5648–5651 (2011).
[45]A. Abragam, *Principles of Nuclear Magnetic Resonance* (Oxford University Press, New York, 1961).
[46]See supplementary material at http://dx.doi.org/10.1063/1.4738761 for a detailed derivation of the DNP parameters for the zero quantum case.